Waves on a columnar vortex in a strongly stratified fluid

Paul Billant[1] and Stéphane Le Dizès[2]

[1]*Laboratoire d'Hydrodynamique (LADHYX), CNRS, Ecole Polytechnique, Palaiseau Cedex F-91128, France*
[2]*Institut de Recherche sur les Phénomènes Hors Équilibre, CNRS, 49, rue F. Joliot-Curie,*
Marseille F-13013, France

This paper investigates the discrete bounded waves sustained by a vertical columnar Rankine vortex in a strongly stratified fluid. We show that these waves are very different from their well-known counterpart in homogeneous fluid (Kelvin vortex waves); they exist only for nonzero azimuthal wavenumber m, their frequency lies in the interval $[0, m\Omega]$ (Ω is the angular velocity in the vortex core) and they are unstable because of an outward radiation from the vortex. The instability mechanism is explained in terms of an over-reflection phenomenon by means of a Wentzel–Kramers–Brillouin–Jeffreys analysis for large axial wavenumber. © *2009 American Institute of Physics*. [doi:10.1063/1.3248366]

I. INTRODUCTION

The discrete waves sustained by a columnar vortex in homogeneous fluids have been described more than one century ago by Kelvin.[1–3] These waves, which are nowadays called Kelvin vortex waves,[4] consist for short axial wavelength in inertial waves due to the vortex rotation and confined to the vortex core. Kelvin considered a Rankine vortex profile (solid body rotation within the vortex core and potential flow outside) and it is only recently that the case of a continuous vortex profile, the Lamb–Oseen vortex, has been analyzed thoroughly.[5] The main difference with the Rankine vortex is the presence of singularities at the radius where the angular phase velocity of the wave equals the angular velocity of the vortex. Some of the Kelvin vortex waves are thus damped by critical layers. The Kelvin vortex waves are involved in the instabilities induced by vortex interactions such as the Crow instability[6] or the elliptic instability[7] in homogeneous fluids. These two instabilities deform the vortex sinuously. They can be understood as a resonance between either long- or short-axial wavelength Kelvin vortex waves with azimuthal wavenumber $m=1$ and the strain field exerted by a companion vortex.

When there is a strong stable stratification along the vortex axis, the Crow instability is inhibited but another instability called zigzag instability occurs.[8] The zigzag instability bends columnar vortices as a whole like the Crow instability and can be also understood as a resonance between the strain and a long-wavelength bending wave.[9] Le Dizès[10] further investigated the effect of a strong stratification on the steady bending waves with short-axial wavelength involved in the elliptic instability. Few studies also considered the general characteristics of the waves sustained by a columnar vertical vortex in the presence of a stable stratification. This configuration is very different from the case of a homogeneous fluid since wavelike motions, i.e., local inertia-gravity waves, are not only confined to the vortex core but can occur everywhere in the fluid. Miyazaki and Fukumoto[11] studied the properties of the axisymmetric waves in the case of a Lamb–Oseen vortex. They have shown that bounded axisymmetric

waves no longer exist when the stratification is strong. The term "bounded" is used here to mean that the waves are localized in the vorticity region as opposed to "unbounded waves" which spread over the whole flow field. However, Schecter and Montgomery[12,13] found that nonaxisymmetric bounded waves can exist in a strongly stratified and rotating fluid and that they are unstable because of gravity wave emission. This paradoxical instability is similar to the radiative instability of the Rankine vortex in a compressible fluid[14] or in shallow water.[15] Schecter and Montgomery[12,13] have further shown that the growth rate of the radiative instability is reduced when a critical layer is present at a radius where the gradient of the vorticity is nonzero. Gravity wave emission has also been investigated on various vortex configurations in stratified and rotating fluids.[16–19]

The study of Schecter and Montgomery[12] for the case of a continuously stratified fluid focuses on the instability mechanism and describes only the most unstable waves. However, a thorough investigation of all the discrete waves of a columnar vertical vortex in a continuously stratified fluid has not been yet carried out. This is the purpose of the present paper in the simple case of the Rankine vortex profile. The problem will be solved numerically but interestingly, some analytical results can be derived in the case of this profile. Moreover, explicit expressions for the dispersion relation of the waves will be provided through asymptotics.

The paper is organized as follows: the problem is formulated in Sec. II. The case of axisymmetric waves and steady waves are first treated analytically in Sec. III. The general case is investigated numerically in Sec. IV. Two asymptotic analyses are then performed for large vertical wavenumber (Sec. V) and for small frequency or small vertical wavenumber (Sec. VI).

II. PROBLEM FORMULATION

We consider an axisymmetric vertical vortex with velocity components $(0, U_\theta(r), 0)$ in cylindrical coordinates (r, θ, z) with z as the vertical coordinate. The fluid is assumed inviscid and stably stratified with a constant Brunt–

Väisälä frequency N. An axisymmetric columnar (i.e., two-dimensional) vortex is steady in such fluid since stratification affects only three-dimensional motions. We subject this basic flow to infinitesimal three-dimensional perturbations of velocity $\tilde{u}$, pressure $\tilde{p}$, and density $\tilde{\rho}$ written in the form

$$[\tilde{u},\tilde{p},\tilde{\rho}](r,\theta,z,t) = [u(r),p(r),\rho(r)]e^{-i\omega t+ikz+im\theta} + \text{cc},$$

where cc denotes the complex conjugate, ω is the frequency, k is the vertical wavenumber, and m is the azimuthal wavenumber. The linearized equations of momentum, density conservation, and continuity under the Boussinesq approximation for the perturbation quantities read

$$isu_r - 2\frac{U_\theta}{r}u_\theta = -\frac{1}{\rho_0}\frac{dp}{dr}, \tag{1}$$

$$isu_\theta + \zeta u_r = -\frac{im}{r}\frac{p}{\rho_0}, \tag{2}$$

$$isu_z = -ik\frac{p}{\rho_0} - \frac{g}{\rho_0}\rho, \tag{3}$$

$$is\rho = N^2\frac{\rho_0}{g}u_z, \tag{4}$$

$$\frac{1}{r}\frac{dru_r}{dr} + i\frac{m}{r}u_\theta + iku_z = 0, \tag{5}$$

where $s=-\omega+mU_\theta/r$ is the Doppler-shifted frequency, $\zeta=(1/r)d(rU_\theta)/dr$ is the axial vorticity of the vortex, g is the gravity, and ρ_0 is a constant reference density. From Eqs. (1)–(4), each velocity component can be easily expressed in terms of the pressure. Then, Eq. (5) gives a single equation for p which can be conveniently further written in terms of $\psi=p/s$:

$$\frac{1}{r}\frac{d}{dr}\left(r\frac{d\psi}{dr}\right) + \frac{\Delta}{s^2}\left(\frac{s^2}{\Delta}\right)'\frac{d\psi}{dr}$$
$$+ \left[\frac{m\Delta}{rs}\left(\frac{\zeta}{\Delta}\right)' - \frac{m^2}{r^2} - k^2\frac{\Delta}{N^2-s^2}\right]\psi = 0, \tag{6}$$

where primes denote differentiation with respect to r, $\Delta=\phi-s^2$, and $\phi=(1/r^3)(r^2U_\theta^2)'$ is the Rayleigh discriminant. Because of the symmetry, $\omega(k,m)=\omega(-k,m)=-\omega^*(-k,-m)$, there is no loss of generality in taking both k and m positive.

In the following, we consider a Rankine vortex profile: $U_\theta=\Omega r$ for $r<R$ and $U_\theta=\Omega R^2/r$ for $r>R$, where Ω is the rate of solid body rotation in the core. In this case, the terms with a prime in Eq. (6) are identically zero for all r. Furthermore, the fluid is assumed to be strongly stratified, i.e., $\Omega\ll N$. We also assume *a priori* that the frequency of the waves is of the same order as the angular velocity of the vortex: $\omega=O(\Omega)$. These two hypotheses allow us to approximate the last term of Eq. (6) as $k^2\Delta/(N^2-s^2)\approx k^2\Delta/N^2$. This is equivalent to assume the hydrostatic balance along the vertical. A convenient consequence is that the problem no longer depends on k and N separately but only through the rescaled wavenumber $\tilde{k}=k/N$ because of the self-similarity

of strongly stratified fluids.[20] Besides, it implies that there is no critical point where $|s|=N$. Under these assumptions, Eq. (6) simplifies to

$$\frac{1}{r}\frac{d}{dr}\left(r\frac{d\psi}{dr}\right) - \frac{m^2}{r^2}\psi + \tilde{k}^2(s^2-\phi)\psi = 0, \tag{7}$$

with $\phi=4\Omega^2$ for $r<R$ and $\phi=0$ for $r>R$. The full problem (i.e., without the hydrostatic approximation) will be briefly discussed in Sec. VII.

The boundary conditions impose that the perturbation is nonsingular at $r=0$ and decays or radiates energy outward as $r\to\infty$. At the boundary of the vortex core $r=R$, the kinematic and dynamic conditions require that the radial velocity and pressure of the perturbation are continuous, respectively. These two conditions can be combined to give

$$s(R)^2\frac{\psi_i'(R)}{\psi_i(R)} + 2ms(R)\frac{\Omega}{R} = (s(R)^2-4\Omega^2)\frac{\psi_o'(R)}{\psi_o(R)}, \tag{8}$$

where ψ_i and ψ_o denote the solution of Eq. (7) for $r<R$ and $r>R$, respectively.

Inside the vortex core $(r<R)$, Eq. (7) can be solved analytically:

$$\psi_i(r) = CJ_m(\tilde{k}\sqrt{s^2-4\Omega^2}r) \quad \text{when} \quad s^2 \neq 4\Omega^2,$$
$$\psi_i(r) = Cr^m \quad \text{when} \quad s^2 = 4\Omega^2, \tag{9}$$

where J_m is the Bessel function of the order of m of the first kind and C is a constant. The sign of the square root is chosen so that $\text{Re}(\sqrt{s^2-4\Omega^2})>0$. When ω is purely real, the solution (9) is oscillatory in the radial direction when $\omega<(m-2)\Omega$ or $\omega>(m+2)\Omega$ and exponentially growing with r otherwise.

In contrast, the solution of Eq. (7) outside the vortex core $(r>R)$ cannot be found analytically[21] except for three particular cases: $m=0$, $\omega=0$, and $k=0$. The last case corresponds to the simple two-dimensional limit for which the dispersion relation is $\omega=(m-1)\Omega$ (See Ref. 2). The first two cases are nontrivial and are investigated in the next section. The general results for arbitrary frequencies and wavenumbers obtained from the numerical integration of Eq. (7) are presented in Sec. IV.

III. ANALYTICAL RESULTS

A. Axisymmetric wave: *m=0*

For $m=0$, Eq. (7) for $r>R$ reduces to a Bessel equation whose general solution can be expressed in terms of Hankel functions $H_0^{(1)}(\tilde{k}\omega r)$ and $H_0^{(2)}(\tilde{k}\omega r)$ or Bessel functions $J_0(\tilde{k}\omega r)$ and $Y_0(\tilde{k}\omega r)$. However, no combination of these solutions satisfies the condition that it must be an outgoing wave for large r for all values of $\arg(\omega)$. For this reason, we introduce a new family of Hankel functions $\tilde{H}_m^{(1)}(z)$ defined by

$$\widetilde{H}_m^{(1)}(z) = \begin{cases} H_m^{(1)}(z), & -\dfrac{\pi}{2} < \arg(z) < \pi, \\[2ex] -H_m^{(1)}(ze^{2i\pi}) = H_m^{(1)}(z) + (1 + e^{-2im\pi})H_m^{(2)}(z), & -\pi \le \arg(z) < -\dfrac{\pi}{2}, \\[2ex] \dfrac{1}{2}(H_m^{(1)}(z) - H_m^{(1)}(ze^{2i\pi})), & \arg(z) = -\dfrac{\pi}{2}, \end{cases} \tag{10}$$

which specifically satisfies this property (see Ref. 22). For $m=0$, the solution of Eq. (2) for $r>R$ can then be written as

$$\psi_o = D\widetilde{H}_0^{(1)}(\widetilde{k}\omega r), \tag{11}$$

where D is a constant. Equation (8) gives then the dispersion relation

$$\widetilde{\omega}\frac{J_1(\kappa\sqrt{\widetilde{\omega}^2-4})}{J_0(\kappa\sqrt{\widetilde{\omega}^2-4})} = \sqrt{\widetilde{\omega}^2-4}\,\frac{\widetilde{H}_1^{(1)}(\kappa\widetilde{\omega})}{\widetilde{H}_0^{(1)}(\kappa\widetilde{\omega})}, \tag{12}$$

where $\kappa=\widetilde{k}\Omega R$ and $\widetilde{\omega}=\omega/\Omega$. This dispersion relation has an infinite number of solutions ω for a given value of κ. Each value of ω can be found in the vicinity of a zero of the Bessel function $J_1(\kappa\sqrt{\widetilde{\omega}^2-4})$, i.e., in the frequency range $|\omega_r| > 2\Omega$, where $\omega_r = \mathrm{Re}(\omega)$. However, the corresponding growth rate $\omega_i = \mathrm{Im}(\omega)$ is always negative implying that the eigenfunction (11) grows exponentially with r and becomes infinite as $r \to \infty$. Therefore, these modes cannot be considered as normal modes although they could have some physical significance for transient dynamics.[13,23] This conclusion is in agreement with the findings of Miyazaki and Fukumoto[11] who have shown that bounded axisymmetric waves can exist only when $N < 2\Omega$.

B. Steady waves: $\omega=0$

When $\omega=0$ and $m \ge 1$, the solution of Eq. (7) for $r>R$ can be found analytically in the form

$$\psi_o = DJ_m\left(\kappa m\frac{R}{r}\right) + EY_m\left(\kappa m\frac{R}{r}\right), \tag{13}$$

where (D,E) are constants and Y_m is the Bessel function of second type of order m. We impose $E=0$ in order that the perturbation decays as $r \to \infty$. Inserting Eqs. (13) and (9) in (8) yields the following dispersion relations:

$$\sqrt{3}\kappa\frac{I_1'(\sqrt{3}\kappa)}{I_1(\sqrt{3}\kappa)} + 2 = 3\kappa\frac{J_1'(\kappa)}{J_1(\kappa)}, \quad \text{for } m=1,$$

$$J_2(2\kappa) = 0, \quad \text{for } m=2, \quad \text{and} \tag{14}$$

$$m\sqrt{m^2-4}\kappa\frac{J_m'(\sqrt{m^2-4}\kappa)}{J_m(\sqrt{m^2-4}\kappa)} + 2m = (4-m^2)\kappa\frac{J_m'(\kappa m)}{J_m(\kappa m)},$$

for $m \ge 3$, where we used the identity $J_1(i\sqrt{3}\kappa)=iI_1(\sqrt{3}\kappa)$ with I_1 as the modified Bessel function of first kind of order one. For each m, there exists an infinity of values of κ satis-

fying these relations. The first roots are listed in Table I for $m=1$ and $m=3$. For $m=1$, there is a root between each zero $j_{i,m}$ of the Bessel function J_m. For $m=2$, the roots are simply given by $j_{i,m}/2$. For $m \ge 3$, there is a root between each of the values: $j_{i,m}/m$ or $j_{i,m}/\sqrt{m^2-4}$ sorted by ascending order.

The profiles of the pressure eigenfunction $p(r)$ of the first three modes for $m=1$ are presented in Fig. 1(a). The difference between these eigenfunctions is the number of nodes n_o outside the vortex core whereas the eigenfunction is evanescent inside. This is the opposite of the case of a homogeneous fluid for which the eigenfunction oscillates in the core and is evanescent outside. For $m \ge 3$, the eigenmode has a wavelike profile both inside and outside the vortex core [Fig. 1(b)]. Each mode is then distinguished by the inner number n_i and outer number n_o of nodes as indicated in Table I.

IV. NUMERICAL RESULTS

In the general case, the solution of Eq. (7) outside the vortex core needs to be computed numerically. The integration is started at a large radius, $r \gg \sqrt{m\Omega/|\omega|}$, for which $s \approx -\omega$. The solution of Eq. (7) which describes an outgoing wave is then: $\psi_o \sim D\widetilde{H}_m^{(1)}(\widetilde{k}\omega r)$, where $\widetilde{H}_m^{(1)}$ has been defined in Eq. (10). Starting from this asymptotic solution with a trial value for ω, we integrate inward to the radius R. A standard root-finding algorithm is then employed to search the values of ω satisfying Eq. (8).

The frequency $\omega_r = \mathrm{Re}(\omega)$ of the waves for $m=1$ are shown on Fig. 2(a). There is an infinite number of branches, each starting from the analytical points for $\omega=0$ indicated by

TABLE I. First roots of the dispersion relation (14) of steady waves ($\omega=0$) for $m=1$ and $m=3$. The numbers n_i and n_o indicate the number of nodes of the eigenfunction inside and outside the vortex core, respectively.

$m=1$		$m=3$	
κ	(n_i,n_o)	κ	(n_i,n_o)
0	(0,0)	1.785	(0,0)
4.740	(0,1)	2.435	(0,1)
7.976	(0,2)	3.116	(1,1)
11.157	(0,3)	3.745	(1,2)
14.320	(0,4)	4.348	(1,3)
17.476	(0,5)	5.006	(2,3)
20.627	(0,6)	5.565	(2,4)
23.776	(0,7)	6.232	(3,4)
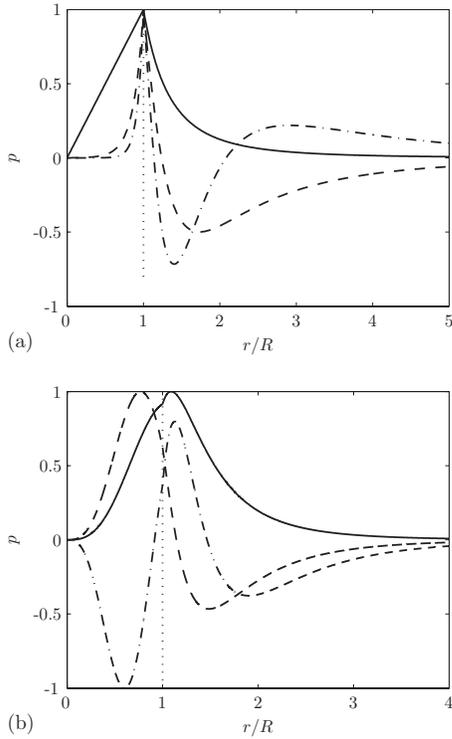
FIG. 1. Eigenfunctions $p(r)$ of steady waves ($\omega=0$) for $m=1$ (a) and $m=3$ (b). For each case, the first three modes listed in Table I are plotted. The vertical dotted line indicates the boundary of the vortex core.

FIG. 2. Frequency $\text{Re}(\omega)/\Omega$ (a) and growth rate $\text{Im}(\omega)/\Omega$ (b) of the waves with azimuthal wavenumber $m=1$ as a function of the rescaled vertical wavenumber $\tilde{k}R\Omega$. Only the sixth first branches are shown. The square symbols in (a) represent the analytical solution for $\omega=0$.

square symbols. As the vertical wavenumber increases, the frequency increases and asymptotes to a value equal to Ω. As seen in Fig. 3, the associated eigenfunction exhibits a decaying wave train whose wavelength decreases as k increases. Figure 2(b) shows that these waves have all a positive growth rate $\omega_i=\text{Im}(\omega)$ meaning that they are unstable. As found by Schecter and Montgomery,[12] the first branch, i.e., the branch deriving from the two-dimensional dispersion relation, $\omega=(m-1)\Omega$, is the most unstable. The maximum growth rate $\omega_i\approx0.06\Omega$ is reached around $\kappa\approx5$. The next section will explain the physical mechanism of this instability by means of a Wentzel–Kramers–Brillouin–Jeffreys (WKBJ) analysis for large wavenumber. Note that the branches can be continued for $\omega_r<0$. However, they are stable ($\omega_i<0$) so that the eigenmodes are unbounded as $r \to\infty$.

The case $m=2$ is qualitatively similar to $m=1$ (Fig. 4). All the branches start from the analytical points for zero frequency except the first branch which originates at $k=0$ from the two-dimensional dispersion relation $\omega=(m-1)\Omega$. The frequency for each branch then increases with the vertical wavenumber up to $\omega=m\Omega$. The first branch is again the most unstable in agreement with Ref. 12. Its maximum growth rate is slightly larger than for $m=1:\text{Im}(\omega)\approx0.08\ \Omega$.

When $m=3$ [Fig. 5(a)], a slightly more complicated behavior is observed. The branches look more closely spaced in the frequency range $0<\omega_r<\Omega$ than in the interval $\Omega<\omega_r<3\Omega$ and some of the branches seem to merge (but do not) around the frequency Ω. For example, the third branch first

saturates at $\omega_r=\Omega$ and then, on the point of colliding the fourth branch, it starts to reincrease to $\omega_r=3\Omega$. This is related to the fact that the eigenmode has not the same structure in the vortex core for these two frequency intervals. Since $\omega_i\ll\omega_r$, the solution (9) in the vortex core is mainly oscillatory for $\omega_r<(m-2)\Omega$ while it is mainly evanescent when $(m-2)\Omega<\omega_r<m\Omega$. The complexity of the eigenfunction and the possible number of branches for a given vertical wavenumber are therefore reduced in the second interval compared to the first. The growth rate is always positive [Fig. 5(b)] but the curves have several local maxima owing to the complicated evolution of the frequency.

For arbitrary azimuthal wavenumber m, the frequency lies in the interval $0<\omega_r<m\Omega$ with two distinct subranges: when $\omega_r<(m-2)\Omega$, the eigenmode is wavelike in the vortex core whereas it is evanescent otherwise. These waves are retrograde since they would appear to rotate in the opposite direction for an observer moving with the fluid, This implies that there always exists a radius where the angular phase velocity ω_r/m is equal to the angular velocity of the vortex. This is a key property to understand the mechanism of these waves as shown in the next section.

V. INSTABILITY MECHANISM

The physical mechanism of the waves can be understood by means of a WKBJ analysis for large rescaled vertical wavenumber $\tilde{k}$ following Le Dizès and Billant.[24] In this limit, the WKBJ approximation of the solution of Eq. (7) for $r>R$ is
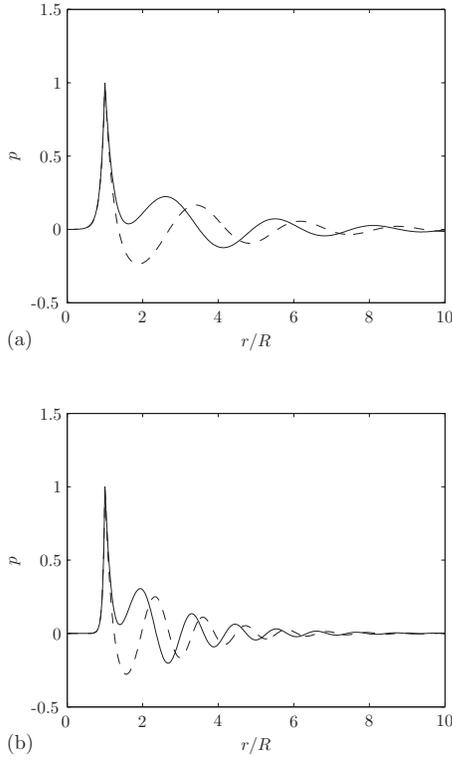
FIG. 3. Eigenfunction $p(r)$ of the first branch for $m=1$ and for $\kappa=5$ (a) and $\kappa=10$ (b). The solid and dashed lines show the real and imaginary parts, respectively.

FIG. 4. Similar to Fig. 2 except for $m=2$. In addition, the dashed lines show the first two branches for a finite Brunt–Väisälä frequency: $N=2.1\Omega$ (i.e., without the hydrostatic approximation).

$$\psi_o \sim \frac{1}{\sqrt{-rs}}[Ae^{i\tilde{k}\theta(r)} + Be^{-i\tilde{k}\theta(r)}], \quad \text{with}$$

$$\theta(r) = \int_r^{r_t} s(u)du, \tag{15}$$

where (A,B) are constants and the radius r_t will be defined below. These two approximations can be identified with waves propagating inward and outward in the radial direction. Since $s\approx -\omega$ for $r\rightarrow\infty$, the phase velocity in the radial direction of the first term of Eq. (15) is positive for large r: $v_\phi = \omega_r/l_r \approx 1/\tilde{k}$, where l_r is the local radial wavenumber, $l_r = \tilde{k}\,Re(\partial\theta/\partial r) = -\tilde{k}\,Re(s) \approx \tilde{k}\omega_r$. The radial component of the group velocity, $v_g = \partial\omega_r/\partial l_r = 1/\tilde{k}$, is also positive. Conversely, the second term of Eq. (15) corresponds to a wave with negative group velocity. In order to have only an outgoing wave for $r\rightarrow\infty$, we therefore impose $B=0$. The WKBJ approximations break down at the so-called turning point where $\theta'(r)=0$. In the case of Eq. (15), this occurs at the radius $r_t = R\sqrt{m\Omega/\omega}$, where $s=0$, i.e., at the critical radius where the azimuthal phase velocity ω_r/m is equal to the angular velocity of the vortex. Since ω has a small positive imaginary part, r_t is slightly off the real r-axis but its real part is always in the interval $[R,\infty[$ because $0<\omega_r<m\Omega$. Near r_t, Eq. (7) reduces at leading order to

$$\frac{\partial^2\psi}{\partial\tilde{r}^2} + \tilde{r}^2\psi + O\left(\frac{1}{q^{1/4}}\right) = 0, \tag{16}$$

where $\tilde{r} = R\sqrt{2\tilde{k}m\Omega/r_t^3}(r-r_t)$ and $q = \tilde{k}^2\omega m\Omega R^2$. This equation is valid only for $\omega\neq 0$ and sufficiently large

wavenumber such that $q\gg 1$. The solution which matches Eq. (15) for $\tilde{r}\rightarrow\infty$ with $-\pi/2<\arg(\tilde{r})<\pi$ is $\psi_o = aD_{-1/2}(\sqrt{2}e^{-i\pi/4}\tilde{r})$, where $D_{-1/2}$ is a parabolic cylinder function and $a = A\exp(-i\pi/8)[\tilde{k}/(r_t\omega)]^{1/4}$. From the behavior of this solution for $\tilde{r}\rightarrow\infty$ with $\pi/2<\arg(\tilde{r})<3\pi/2$, we deduce the matching WKBJ approximation for $r<r_t$ (see Bender and Orszag[25] for details),

$$\psi_o \sim \frac{1}{\sqrt{rs}}[Ce^{i\tilde{k}\theta(r)} + De^{-i\tilde{k}\theta(r)}], \tag{17}$$

where $C=-iA$ and $D=\sqrt{2}A$. The phase velocity in the radial direction of the first term is now negative $v_\phi = -\omega_r/[\tilde{k}\,Re(s)]$ since $\omega_r>0$ and $Re(s)>0$ for $r<r_t$ but the group velocity $v_g = 1/\tilde{k}$ is still positive, i.e., the energy is going outward. Conversely, the group velocity of the second term of Eq. (17) is negative. Hence, the first and second terms of Eq. (17) correspond, respectively, to the incident wave and to the reflected wave while Eq. (15) is the transmitted wave. The reflection and transmission coefficients at the critical radius r_t are therefore $\mathcal{R}=|D^2/C^2|=2$ and $\mathcal{T}=|A^2/C^2|=1$. Strikingly, even if some of the energy is transmitted through the critical radius and radiates away, the reflection coefficient is larger than unity, i.e., the reflected wave has a larger amplitude than the incident wave. This over-reflection process at the critical radius has been shown to be at the origin of many instabilities by Lindzen and co-workers (see, for example, Refs. 26 and 27). Indeed, if there is a second boundary for $r<r_t$, the over-reflected wave will be reflected back toward the over-reflecting region. When this "reflected over-reflected" wave is in phase with the in-

FIG. 5. Similar to Fig. 2 except for $m=3$.

FIG. 6. Frequency (a) and growth rate (b) for $m=1$ as a function of the rescaled vertical wavenumber $\tilde{k}R\Omega$. Comparison between the exact results (solid lines) and the WKBJ predictions: Eq. (19) (dotted lines) and Eqs. (20) and (21) (dashed lines).

cident wave and if the product of reflection and over-reflection exceed unity, we have a resonant amplification of the waves and thus an instability. In the present case, the boundary condition (8) at $r=R$ implies $|C|=|D|$ when ω is purely real. Thus, the reflection coefficient at $r=R$ is unity so that an instability will occur when the phase condition is satisfied.

An approximate dispersion relation for large vertical wavenumber can be obtained by inserting Eq. (17) in Eq. (8),

$$\tan\left(\tilde{k}\theta(R) - \frac{\pi}{4} + \frac{i}{4}\ln 2\right)$$
$$= -\frac{s(R)}{\sqrt{4\Omega^2 - s(R)^2}}\frac{J'_m(\tilde{k}R\sqrt{s(R)^2 - 4\Omega^2})}{J_m(\tilde{k}R\sqrt{s(R)^2 - 4\Omega^2})} + O\left(\frac{1}{\tilde{k}R}\right). \tag{18}$$

Expanding this dispersion relation in powers of $\tilde{k}R$ yields an explicit expression for ω,

$$\omega = m\Omega - 2\sqrt{\frac{m\Omega\mu}{\tilde{k}R}} + \frac{\mu+m}{\tilde{k}R} + O[(\tilde{k}R)^{-3/2}], \tag{19}$$

where $\mu = (\pi/4) - (i/4)\ln 2 + n\pi$ and n is a non-negative integer. As seen in Fig. 6 for the azimuthal wavenumber $m=1$, the asymptotic formula (19) (represented by dotted lines) gives a very good approximation of the exact frequency (solid lines) for large wavenumbers but it diverges at low wavenumbers. Since the growth rate is small compared to the frequency, $\omega_i \ll \omega_r$, it turns out that a better approximation can be obtained by expanding Eq. (18) with ω_i. This

gives at zeroth order in ω_i, an explicit relation for $\tilde{k}$ as a function of ω_r,

$$\tilde{k}R = \frac{\frac{\pi}{4} - \beta_r + n\pi}{(\sqrt{\omega_r} - \sqrt{m\Omega})^2}, \tag{20}$$

where $\tan\beta_r = (m\Omega - \omega_r)/\sqrt{4\Omega^2 - (m\Omega - \omega_r)^2}$. The next order gives the growth rate

$$\omega_i = -\frac{i}{4}\frac{\ln 2}{\tilde{k}R(1 - \sqrt{m\Omega/\omega_r}) - 1/\sqrt{4\Omega^2 - (m\Omega - \omega_r)^2}}. \tag{21}$$

These predictions are shown by dashed lines in Fig. 6. The frequency predicted by Eq. (20) is almost superposed to the exact frequency for all wavenumbers (solid lines) except for the first branch [Fig. 6(a)] and for small frequency. The departure at low frequency can be better seen in Fig. 7 which shows a close view of this region for $m=1$ and $m=2$. The growth rate is also in very good agreement with the exact results except for the beginning of the curves and for the first branch [Fig. 6(b)]. The dispersion relation (18) can be also solved directly but the results are almost identical to those given by Eqs. (20) and (21) in the case of the azimuthal wavenumbers $m=1$ and $m=2$.

Finally, it is interesting to note that, when $\omega_r > m\Omega$ or $\omega_r < 0$, the WKBJ approximation (15) is valid throughout the interval $[R, \infty[$. Inserting this approximation in Eq. (8) gives a dispersion relation whose solutions exist in the frequency intervals: $\omega_r > (m+2)\Omega$ and $\omega_r < (m-2)\Omega$. However, the
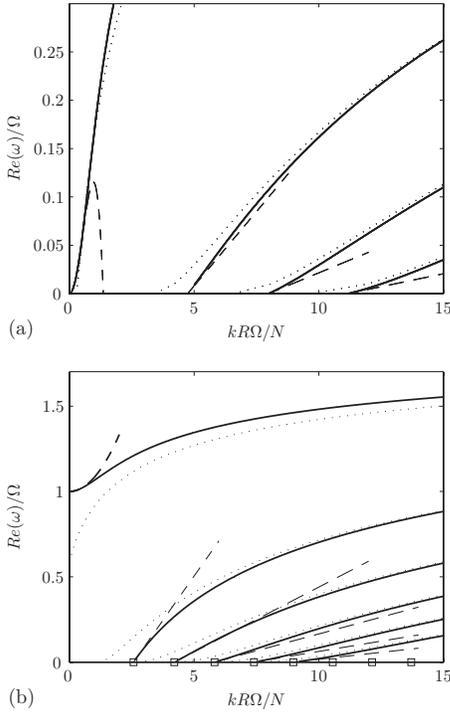
FIG. 7. Frequency for $m=1$ (a) and $m=2$ (b) as a function of the rescaled vertical wavenumber $\tilde{k}R\Omega$. Comparison between the exact results (solid lines) and the asymptotic results for small ω or small $\tilde{k}$ (dashed lines). The WKBJ predictions given by Eq. (20) are also indicated by dotted lines.

corresponding growth rates ω_i are always negative meaning that the eigenfunctions are unbounded as $r\to\infty$ like for $m=0$.

VI. ASYMPTOTIC RESULTS FOR SLOW MODES AND LONG-WAVELENGTH MODES

The WKBJ analysis presented in the previous section is only valid when $q=\tilde{k}^2\omega m\Omega R^2\gg 1$ and is therefore unable to describe the limits of small frequency or small vertical wavenumber. In the first case, $\omega\to 0$ with $\tilde{k}$ arbitrary, the solution of Eq. (7) for $r>R$ can be easily found in two distinct regions: for $r\ll 1/(\tilde{k}\omega)$ and for $\tilde{k}m\Omega R^2\ll r$. These two solutions will be matched when the parameter q is small. In the first region [i.e., for $r\ll 1/(\tilde{k}\omega)$], Eq. (7) approximates to

$$r\frac{\partial}{\partial r}\left(r\frac{\partial\psi}{\partial r}\right)-\left[m^2+2q-\frac{(\tilde{k}m\Omega R^2)^2}{r^2}\right]\psi+O[(\tilde{k}\omega r)^2]=0.$$
(22)

The solution is

$$\psi_1=A_1J_a(u)+B_1Y_a(u)+O(q^2/u^2),$$
(23)

where $u=\tilde{k}m\Omega R^2/r$, $a=\sqrt{m^2+2q}$, and (A_1,B_1) are constants. In the second region (i.e., for $\tilde{k}m\Omega R^2\ll r$), Eq. (7) reduces to

$$r\frac{\partial}{\partial r}\left(r\frac{\partial\psi}{\partial r}\right)-(m^2+2q-\tilde{k}^2\omega^2 r^2)\psi+O[(\tilde{k}m\Omega R^2/r)^2]=0.$$
(24)

The solution which describes an outgoing wave for $r\to\infty$ is

$$\psi_2=A_2\tilde{H}_a^{(1)}(\tilde{k}\omega r)+O[(\tilde{k}m\Omega R^2/r)^2],$$
(25)

where $\tilde{H}_a^{(1)}$ has been defined in Eq. (10) and A_2 is a constant.

When q is small, ψ_1 and ψ_2 should match in the overlap region: $\tilde{k}m\Omega R^2=q/(\tilde{k}\omega)\ll r\ll 1/(\tilde{k}\omega)$. In this region, when $Im(\omega)>0$, ψ_1 and ψ_2 approximate at leading order to

$$\psi_1\sim A_1\left[\frac{1}{m!}\left(\frac{\tilde{k}m\Omega R^2}{2r}\right)^m+\cdots\right]$$
$$-B_1\left[\frac{(m-1)!}{\pi}\left(\frac{\tilde{k}m\Omega R^2}{2r}\right)^{-m}+\cdots\right],$$
(26)

$$\psi_2\sim A_2\left[\frac{1}{m!}\left(\frac{\tilde{k}\omega r}{2}\right)^m+\cdots\right]$$
$$-iA_2\left[\frac{(m-1)!}{\pi}\left(\frac{\tilde{k}\omega r}{2}\right)^{-m}+\cdots\right].$$
(27)

Thus, ψ_1 and ψ_2 match at leading order if

$$A_1/A_2=-i\frac{m!\,(m-1)!}{\pi}\left(\frac{4}{q}\right)^m+O(q^{1-m}),$$
(28)

$$B_1/A_2=-\frac{\pi}{m!\,(m-1)!}\left(\frac{q}{4}\right)^m+iO(q^m).$$
(29)

The matching at this order does not allow us to obtain the last term of Eq. (29) (which is imaginary) because it would be necessary to consider higher order terms in Eqs. (26)–(28). Nevertheless the first term of Eq. (29) which is real and also $O(q^m)$ can be obtained because it is the first real term showing up in the matching sequence. Since the magnitude of B_1 is $B_1=O(q^mA_2)=O(q^{2m}A_1)$, we can approximate the real part of the solution in the first region by

$$Re\left(\frac{\psi_1}{A_1}\right)=J_a(u)+O(q^{2m},q^2/u^2).$$

We can further expand the order of the Bessel function: $a=m+(q/m)+O(q^2)$ (see Ref. 22) to obtain an approximation valid up to $O(q)$:

$$Re\left(\frac{\psi_1}{A_1}\right)=J_m(u)+\frac{q}{2m}$$
$$\times\left[\pi Y_m(u)+m!\sum_{n=0}^{m-1}\left(\frac{2}{u}\right)^{m-n}\frac{J_n(u)}{n!\,(m-n)}\right]$$
$$+O(q^2).$$
(30)

In addition, the first imaginary term is significant even if its magnitude is equal or smaller than $O(q^2)$:

$$Im\left(\frac{\psi_1}{A_1}\right)=-\left(\frac{\pi}{m!\,(m-1)!}\right)^2\left(\frac{q}{4}\right)^{2m}Y_m(u)+O(q^{2m+1}).$$
(31)

Inserting this solution in the dispersion relation (8) shows that the frequency of the first branch for $m=1$ is $\omega_r=\Omega(\kappa^2/4-13\kappa^4/96+\cdots)$ and of the form $\omega_r\propto(\kappa-\kappa_0)$ otherwise, where κ_0 is the rescaled wavenumber satisfying

the dispersion relation for $\omega=0$. These asymptotic formulae predict well the beginning of the branches at $\omega=0$ as shown in Fig. 7. They can be useful since the WKBJ predictions depart from the exact results in this regime. We can further deduce from Eq. (31) that the growth rate is at leading order $\omega_i=\Omega\pi\kappa^6/64+\cdots$ for the first branch for $m=1$ and is of the form $\omega_i\propto(\kappa-\kappa_0)^{2m}$ otherwise.

In the case of a small wavenumber $\tilde{k}\to0$ and a finite frequency, the solutions (23) and (25) remain valid but Eq. (23) is then only valid at order $O(1)$. A solution which is valid at order $O(\tilde{k}^2)$ can be easily obtained as an expansion in powers of $\tilde{k}^2$. Matching this solution to Eq. (25) gives

$$\mathrm{Re}\left(\frac{\psi_1}{A_1}\right)=\frac{1}{r^m}\left[1-\tilde{k}^2\left(\omega\Omega R^2\ln r+\frac{\omega^2}{4-4\,m}r^2\right.\right.$$
$$\left.\left.+\frac{(m\Omega R^2)^2}{4(1+m)r^2}\right)+O(\tilde{k}^4)\right],\tag{32}$$

$$\mathrm{Im}\left(\frac{\psi_1}{A_1}\right)=\frac{\pi}{m\,!\,(m-1)!}\left(\frac{\tilde{k}\omega}{2}\right)^{2m}r^m+\cdots,\tag{33}$$

for $m\geq2$. Inserting this solution in Eq. (8) yields the leading three-dimensional correction to the dispersion relation of two-dimensional modes:

$$\omega_r=\Omega\left(m-1+\frac{\kappa^2}{2m(m+1)}+O(\kappa^4)\right),$$
$$\omega_i=\frac{\pi\Omega}{m\,!\,(m-1)!}\left(\frac{\kappa\omega_r}{2\Omega}\right)^{2m}.\tag{34}$$

The asymptotic formula for the frequency is in good agreement with the beginning of the branch originating from the two-dimensional limit as shown in Fig. 7(b) for $m=2$.

VII. CONCLUSIONS

We have shown that a vertical Rankine vortex in a continuously strongly stratified fluid can support a family of nonaxisymmetric discrete bounded waves. For each nonzero azimuthal wavenumber, there is an infinite number of branches with frequency in the range $0<\omega_r<m\Omega$. It is worth noticing that this interval is very different from the frequency range of inertia-gravity waves for a uniformly and unbounded rotating stratified flow: $2\Omega<|\omega_r-m\Omega|<N$. The waves are unstable because of an outward radiation of waves like for vortices in compressible fluid,[14] shallow water fluid,[15] or strongly stratified and rotating fluids.[12,13] The instability is connected to an over-reflection phenomenon at the critical radius where the angular phase velocity of the waves is equal to the angular velocity of the basic vortex. For each azimuthal wavenumber, we observed that the branch which originates from the two-dimensional limit is the most unstable.

For simplicity, we assumed herein a strongly stratified fluid $N\gg\Omega$, i.e., the hydrostatic approximation. In this limit, the results depend on the Brunt–Väisälä frequency only through the rescaled vertical wavenumber $kR\Omega/N$. However, the results remain almost the same when N is finite provided

that $N>|m\Omega|$. As an example, the dashed lines in Fig. 4 shows the first two branches for $m=2$ for the Brunt–Väisälä frequency $N=2.1\Omega$. Strikingly, we see that there is almost no difference with the case $N\gg\Omega$ (solid lines). However, when $N<|m\Omega|$, the waves with frequency in the range $\omega<m\Omega-N$ or $\omega>N$ have a singularity at the radius where $|s|=N$ so that some differences should start to appear. Similar waves have been found in the case of a continuous vortex profile: the Lamb–Oseen vortex.[24]

Since they are all unstable, these waves should affect the dynamics of any isolated columnar vortex in a stratified fluid. When there are several vortices in interaction, these waves could be further destabilized through a resonance with the strain field exerted by companion vortices. In this context, the description of the vortex waves as provided herein is of primary importance since the characteristics of the resulting instabilities (most amplified wavelength, structure of the perturbation) are directly related to the properties of the wave branch that is destabilized. For example, as already mentioned in the Introduction, the Crow and elliptic instabilities of vortex pairs in homogeneous fluids are due, respectively, to the resonance between the strain and the long- and short-axial wavelength vortex waves with azimuthal wavenumber $m=\pm1$. In the same way, the first branch of the vortex waves with azimuthal wavenumber $m=\pm1$ in the case of a strongly stratified fluid can be also destabilized by a strain field.[8,9] This mechanism leads to a long-axial wavelength instability of vortex pairs in stratified fluids, the zigzag instability, which is analogous to the Crow instability in homogeneous fluids. Interestingly, the stability analysis of a vertical vortex pair in a strongly stratified fluid performed by Waite and Smolarkiewicz[28] suggests that there exists a second growth rate peak at larger axial wavenumber than the zigzag instability one's. On the basis of the present results, we can hypothesize that this second peak comes from the destabilization of the second branch of waves with $m=\pm1$. To test this hypothesis, it would be interesting to determine whether or not a strain field can destabilize these wave branches.

[1] L. Kelvin, "Vibrations of a columnar vortex," Philos. Mag. **10**, 155 (1880).

[2] P. G. Saffman, *Vortex Dynamics* (Cambridge University Press, Cambridge, 1992).

[3] M. Rossi, Lec. Notes Phys. **555**, 40 (2000).

[4] The Kelvin vortex waves should not be confused with the other type of Kelvin waves in geophysical fluid dynamics, i.e., the gravitational waves along a boundary in a rotating fluid.

[5] D. Fabre, D. Sipp, and L. Jacquin, "The Kelvin waves and the singular modes of the Lamb–Oseen vortex," J. Fluid Mech. **551**, 235 (2006).

[6] S. C. Crow, "Stability theory for a pair of trailing vortices," AIAA J. **8**, 2172 (1970).

[7] C.-Y. Tsai and S. E. Widnall, "The stability of short waves on a straight vortex filament in a weak externally imposed strain field," J. Fluid Mech. **73**, 721 (1976).

[8] P. Billant and J.-M. Chomaz, "Experimental evidence for a new instability of a vertical columnar vortex pair in a strongly stratified fluid," J. Fluid Mech. **418**, 167 (2000).

[9] P. Otheguy, P. Billant, and J. M. Chomaz, "Theoretical analysis of the zigzag instability of a vertical co-rotating vortex pair in a strongly stratified fluid," J. Fluid Mech. **584**, 103 (2007).

[10] S. Le Dizès, "Inviscid waves on a Lamb-Oseen vortex in a rotating stratified fluid: Consequences on the elliptic instability," J. Fluid Mech. **597**, 283 (2008).

[11]T. Miyazaki and Y. Fukumoto, "Axisymmetric waves on a vertical vortex in a stratified fluid," Phys. Fluids A **3**, 606 (1991).

[12]D. A. Schecter and M. T. Montgomery, "Damping and pumping of a vortex Rossby wave in a monotonic cyclone: Critical layer stirring versus inertia-buoyancy wave emission," Phys. Fluids **16**, 1334 (2004).

[13]D. A. Schecter and M. T. Montgomery, "Conditions that inhibit the spontaneous radiation of spiral inertia-gravity waves from an intense mesoscale cyclone," J. Atmos. Sci. **63**, 435 (2006).

[14]E. Broadbent and D. W. Moore, "Acoustic destabilization of vortices," Philos. Trans. R. Soc. London, Ser. A **290**, 353 (1979).

[15]R. Ford, "The instability of an axisymmetric vortex with monotonic potential vorticity in rotating shallow water," J. Fluid Mech. **280**, 303 (1994).

[16]R. Plougonven and V. Zeitlin, "Internal gravity wave emission from a pancake vortex: An example of wave-vortex interaction in strongly stratified flows," Phys. Fluids **14**, 1259 (2002).

[17]D. A. Schecter and M. T. Montgomery, "Waves in a cloudy vortex," J. Atmos. Sci. **64**, 314 (2007).

[18]D. Hodyss and D. S. Nolan, "The Rossby-inertia-buoyancy instability in baroclinic vortices," Phys. Fluids **20**, 096602 (2008).

[19]D. A. Schecter, "The spontaneous imbalance of an atmospheric vortex at high Rossby number," J. Atmos. Sci. **65**, 2498 (2008).

[20]P. Billant and J.-M. Chomaz, "Self-similarity of strongly stratified inviscid flows," Phys. Fluids **13**, 1645 (2001).

[21]Note that Eq. (7) can be put into the form of a modified Mathieu equation with the change of variable $u = \ln(r^2 \omega / (m \Omega R^2))/2$. However, this is not very helpful because the modified Mathieu functions are not tabulated for arbitrary parameters.

[22]M. Abramowitz and I. A. Stegun, *Handbook of Mathematical Functions* (Dover, New York, 1965).

[23]P. H. Roberts, "On vortex waves in compressible fluids. I. The hollow-core vortex," Philos. Trans. R. Soc. London, Ser. A **459**, 331 (2003).

[24]S. Le Dizès and P. Billant, "Radiative instability in stratified vortices," Phys. Fluids **21**, 096602 (2009).

[25]C. M. Bender and S. A. Orszag, *Advanced Mathematical Methods for Scientists and Engineers* (McGraw-Hill, New York, 1978).

[26]R. Lindzen, B. Farell, and K. Tung, "The concept of wave overreflection and its application to baroclinic instability," J. Atmos. Sci. **37**, 44 (1980).

[27]R. S. Lindzen and J. W. Barker, "Instability and wave over-reflection in stably stratified shear flow," J. Fluid Mech. **151**, 189 (1985).

[28]M. L. Waite and P. K. Smolarkiewicz, "Instability and breakdown of a vertical vortex pair in a strongly stratified fluid," J. Fluid Mech. **606**, 239 (2008).